APL Materials

Colossal barocaloric effects in adamantane derivatives for thermal management

Cite as: APL Mater. **10**, 111117 (2022); https://doi.org/10.1063/5.0127667
Submitted: 23 September 2022 • Accepted: 31 October 2022 • Published Online: 16 November 2022

Alejandro Salvatori, Philippe Negrier, Araceli Aznar, et al.

AIP Publishing

Colossal barocaloric effects in adamantane derivatives for thermal management

Cite as: APL Mater. 10, 111117 (2022); doi: 10.1063/5.0127667
Submitted: 23 September 2022 • Accepted: 31 October 2022 •
Published Online: 16 November 2022

View Online Export Citation CrossMark

Alejandro Salvatori,[1] Philippe Negrier,[2] Araceli Aznar,[1] María Barrio,[1] Josep Lluís Tamarit,[1] and Pol Lloveras[1,a)]

AFFILIATIONS

[1] Group of Characterization of Materials, Department of Physics, EEBE and Barcelona Research Center in Multiscale Science and Engineering, Universitat Politècnica de Catalunya, Av. Eduard Maristany 10-14, Barcelona 08019, Catalonia, Spain
[2] Université de Bordeaux, LOMA, UMR 5798, F33400 Talence, France

[a)] **Author to whom correspondence should be addressed:** pol.lloveras@upc.edu

ABSTRACT

Plastic crystals are currently attracting interest because their solid-state caloric functionality could be used to tackle climate change in two critical areas: (i) more environmentally friendly cooling and heating driven by pressure and (ii) passive waste heat management. Here, we suggest that plastic crystals could also be used for active pressure-assisted (i.e., barocaloric) waste heat management. In contrast to the barocaloric cooling/heating cycle, for active barocaloric waste heat management, the hysteresis may not be a constraint and transition temperatures above ambient are usually desired. In contrast to passive waste heat management, the application of pressure can be an advantage to actively control the absorption and delivery of heat by the plastic crystal. Here, we have investigated the pressure-induced caloric response at the first-order phase transitions occurring above room temperature of three plastic crystals derived from adamantane: 1-adamantanol, 2-adamantanol, and 2-methyl-2-adamantanol. Colossal barocaloric effects have been found for two of them under small pressure changes of 50 MPa. This behavior occurs thanks to a colossal transition entropy change and a large transition sensitivity to pressure, which can simultaneously take place due to enormous transition volume changes. The balance between configurational and volumic entropy changes at the transition has also been discussed. For 2-adamantanol, in addition to the transition to the plastic phase, the less energetic triclinic-to-monoclinic transition at lower temperatures has also been analyzed. The transition temperatures above ambient make these compounds suitable for waste heat management and, thanks to a small hysteresis, also for industrial cooling and heat pumping.

I. INTRODUCTION

Plastic crystals can act as solid-state heat sources or sinks due to the release or absorption of very large latent heat associated with a first-order phase transition (FOPT) between ordered and orientationally disordered phases.[1–3] Moreover, the phase transition temperature can be largely tuned by the application of a hydrostatic pressure due to large transition volume changes,[4,5] which, along with the large latent heat, gives rise to colossal barocaloric (BC) effects. These features are currently boosting research in these materials to cope with climate change and pollution because they could offer more environmentally friendly cooling and heat pumping techniques as an alternative to appliances based on the vapor compression cycle that use very high greenhouse hydrofluorocarbons (HFCs).[6] In this technology, used in about 80% of cooling devices, the direct leakage of HFCs to the atmosphere yields 3.5% of total CO2-equivalent emissions, whereas the total impact considering the energy consumption amounts to almost 8% of it. In cooling cycles, barocaloric materials undergoing a FOPT with low transition hysteresis are desired because they allow the FOPT to occur back and forth under relatively small pressure changes and at high frequencies. Additionally, for refrigeration and air conditioning in both household and transport settings, FOPTs close to or below room temperature are required, whereas those above ambient could be appealing for cooling and heating applications not related to human comfort, as in the industrial sector and/or heat engines.

On the other hand, for plastic crystals undergoing FOPTs above ambient, the pressure-assisted caloric functionality could also be used for the recovery and storage of waste heat, which also represents a serious environmental thread. It is estimated that about 70% of all energy produced by mankind is dissipated in the form of heat into the environment, with the corresponding direct warming impact. In industry, waste heat represents 20%–50% of energy consumption, and it is estimated that up to 30% of it could be reused.[7–10] Moreover, most of the waste heat is available below 200 °C, whereas most of the conventional heat recovery technologies require higher temperatures.[11] Given the large room for improvement, a number of initiatives to harvest the waste heat from human origin have arisen, which is viewed as a renewable energy resource. Here, endothermic FOPTs in plastic crystals occurring well below 200 °C, yet above room temperature and therefore inappropriate for household cooling, could offer a solution as heat storage media at such temperatures. The solid-to-solid character of FOPTs in plastic crystals can also be advantageous compared to methods based on the melting of phase change materials (PCMs) because of avoiding drawbacks related to leakage and handling that force their encapsulation.[12] In this sense, plastic crystals have been proposed as an active element to obtain shape-stabilized molten PCMs.[13,14]

Moreover, in contrast to cyclic cooling, the harvesting and storage of heat does not require high operational frequencies, and transition hysteresis can be viewed as a positive feature as it provides greater stability to the heat-storing phase. Very interestingly, the temperatures for both the endothermic FOPT (used to store the heat) and the exothermic FOPT (used for the subsequent delivery of heat when necessary) can be tuned by the application of pressure to adapt to the system requirements and enhance the time period of storage. This method, which has been recently proposed using other types of materials,[15,16] adds flexibility to the conventional passive method, which has been traditionally proposed commonly for thermal energy storage.[14,17]

On the other hand, at least at the theoretical level, it is conceivable that plastic crystals could also be used in the organic Rankine cycle[18] for power production from waste heat as an intermediary to heat the boiling working fluid and/or as an active part by taking advantage of the high vapor pressure and relatively easy sublimation ability.[19]

Stimulated by these potential applicabilities, in this work, we analyze the BC response of three plastic crystals derived from adamantane across their FOPTs. Adamantane [$(CH)_4(CH_2)_6$] is made up by the fusion of four cyclohexane rings that provide the molecule with a highly symmetrical, rigid cage-like structure. Below the melting point at 543 K, adamantane crystallizes in the plastic phase[20] with an fcc structure with Z = 4 molecules per unit cell.[21] Upon further cooling, adamantane undergoes a solid–solid FOPT at 208.6 K toward a tetragonal ordered phase. Simple substitutions at either the 1-(tertiary carbon) or 2-(secondary carbon) positions of adamantane give rise to a rich panoply of materials with different solid-state properties and then with a large variety of FOPT temperatures and enthalpy changes,[22–25] which can be of interest for potential applications that aim to take advantage of the transition. In particular, we study 1-adamantanol, 2-adamantanol, and 2-methyl-2-adamantanol (named hereafter 1Aol, 2Aol, and 2M2Aol, respectively, for short). 1Aol is obtained through the substitution of an H atom attached to the tertiary carbon atom by a hydroxyl group. 2Aol and 2M2Aol are obtained by replacing either one of the two H atoms attached to the secondary carbon atom by a hydroxyl group (2Aol) or two H atoms by methyl and hydroxyl groups (2M2Aol). At high temperatures and below the melting point, 1Aol, 2Aol, and 2M2Aol exhibit a plastic face-centered cubic phase (FCC for short). On cooling, the three compounds undergo a solid–solid transition toward an orientation-ordered phase, which for 1Aol shows a tetragonal structure (T), for 2Aol a monoclinic structure (M), and for 2M2Aol an orthorhombic structure (O). In addition, 2Aol exhibits an additional lower temperature triclinic phase (Tr). The structures of low-temperature ordered phases for 2Aol and 2M2Aol have been reported very recently, whereas those of 1Aol were published a long time ago.[26] To the best of our knowledge, no structural refinement of the plastic phases for the three adamantane derivatives has been reported yet.

Currently, these compounds are used in industry as intermediates for the synthesis of other compounds. In particular, they are used to produce 1,3-adamantanediol,[27] which in turn is used as a raw material to make functional and electronic materials.[28] In addition, 1Aol and 2Aol can be used to synthesize compounds that show analgesic activity and antiviral and antibacterial properties.[29] Moreover, 2M2Aol can be used to produce light-resistant polymers for application in photolithography.[30] In general, adamantane and some derivatives also present medical applications, such as in prophylaxis, as an antiviral, and for Parkinson's treatment.[31–33]

II. MATERIALS AND METHODS

A powdered sample of 1Aol (purity 99%) was purchased from Fluka and used as such, and 2Aol (97%) and 2M2Aol (97%) were purchased from Sigma-Aldrich. For both 2Aol and 2M2Aol, additional purification was performed by two methods: recrystallization from ethanol at room temperature and sublimation at 323 K. The temperature and enthalpy changes related to the III–II and II–I transitions in the purified and purchased samples do not differ significantly. Differential scanning calorimetry measurements were performed using a Q100 thermal analyzer from TA Instruments at different scanning rates in the range 2–10 K min^{-1} with ~5 mg of sample sealed in hermetic Al pans. High-pressure differential thermal analysis measurements were performed using a bespoke calorimeter consisting of a Bridgman pressure cell. Heating ramps were performed by means of a resistive heater at 3 K min^{-1}, whereas cooling ramps were performed in contact with an air stream at ca. ~−1.5 K min^{-1}. A few hundred mg of each sample was encapsulated inside bespoke tin capsules with a perfluorinated fluid (Galden Bioblock Scientist) to remove air bubbles. The pressure transmitting liquid used in the pressure circuit was Therm-240 (Lauda).

High-resolution x-ray powder diffraction (XRPD) for the plastic phases of the three compounds under study and for the tetragonal phase of 1Aol was performed at atmospheric pressure and at different temperatures using an INEL transmission diffractometer with a germanium monochromator, a cylindrical position-sensitive detector (CPS-120), and the Debye–Scherrer geometry, using Cu-$K\alpha_1$ = 1.54056 Å radiation. Powdered samples were introduced into a Lindemann capillary (0.5 mm in diameter), and the temperature was varied using a 700 series Oxford Cryostream Cooler. For 1Aol, x-ray patterns were acquired isothermally between 150 K and 475 K in

order to determine the lattice parameters as a function of temperature and the volume variation at the FOPT. The data were analyzed with Materials Studio software.[34] First, a Pawley fit was performed to find cell parameters, profiles, the zero offset, and asymmetry. Then, a Rietveld refinement was performed, assuming a rigid body molecule. For the tetragonal and plastic phases of 1Aol, the intramolecular distances and angles reported from single crystal diffraction by Amoureux *et al.*[26] were kept. For the plastic phases of 1Aol and 2Aol, the energy minimization Materials Studio Forcite module was used to obtain the intramolecular distances and angles. For the plastic phase of 2M2Aol, the intramolecular distances and angles were kept almost identical to the low-temperature phases reported recently.[35] The obtained R-factors were *Rwp* = 5.23% and *Rp* = 3.68% for the tetragonal phase of 1Aol, *Rwp* = 6.36% and *Rp* = 4.32% for the plastic phase of 1Aol, *Rwp* = 5.20% and *Rp* = 3.90% for the plastic phase of 2Aol, and *Rwp* = 5.40% and *Rp* = 4.00% for the plastic phase of 2M2Aol.

III. RESULTS AND DISCUSSION

A. Characterization of phase transitions and phase diagrams

Isobaric high-pressure differential thermal analyses at selected pressures were performed on heating and cooling for the three compounds 1Aol, 2Aol, and 2M2Aol across both endothermic (T → FCC for 1Aol, Tr → M → FCC for 2Aol, and O → FCC for 2M2Aol) and the corresponding reversing exothermic phase transitions. The signals, shown in Figs. 1(a)–1(c), display calorimetric peaks associated with the aforementioned transitions.

Enthalpy and entropy changes at the transition were calculated from peak integration after baseline subtraction as $\Delta H_t(p) = \int_{T_1}^{T_2} \frac{dQ}{dT} dT$ and $\Delta S_t(p) = \int_{T_1}^{T_2} \frac{1}{T} \frac{dQ}{dT} dT$ [the latter are shown in Figs. 1(d)–1(f)]. Here, temperatures T_1 and T_2 were chosen below and above the transition to properly define the baseline, and $\frac{dQ}{dT} = \frac{\dot{Q}}{\dot{T}}$. The values obtained for ΔH_t and ΔS_t at atmospheric pressure (see Table II) coincide for 2Aol and 2M2Aol with the data published in Ref. 35, whereas for 1Aol, they are in very good agreement with the literature.[36] In plastic crystals, these large transition entropy changes are expected to emerge mainly due to changes in the configurational entropy ΔS_c and in volumic entropy ΔS^V.[37,38] The latter can be estimated as[39,40] $\Delta S^V \sim \frac{\langle \alpha \rangle}{\langle \chi \rangle} \Delta V_t$, where $\langle \alpha \rangle$ and $\langle \chi \rangle$ are the averages of the isobaric thermal expansion and isothermal compressibility of the two phases averaged close to the transition, respectively, and ΔV_t is the volume change at the transition. Values for α and ΔV_t can be found in Tables I and II. As for $\langle \chi \rangle$, we do not have our own data or literature data for these compounds. However, some studies have reported these data for adamantane[41–43] and its halogen derivatives,[44] which have been shown to vary little from each other. From these studies, we have used $\langle \chi \rangle \simeq 0.3\ \mathrm{GPa}^{-1}$ for the three compounds under study.

In turn, the configurational entropy change can be calculated from $\Delta S^c_{i \to f} = RM^{-1} \ln\left(\frac{N_f}{N_i}\right)$ where N_i and N_f refer to the number of possible configurations in the initial and final phases involved

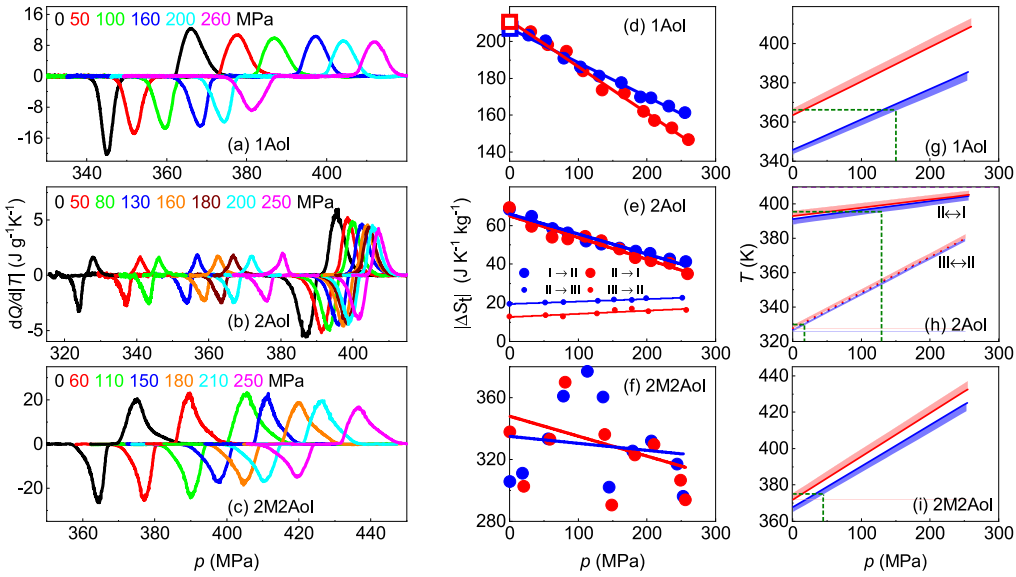

FIG. 1. (a)–(c) Isobaric calorimetry measurements at selected pressures (values at the top) on heating (positive) and cooling (negative) for (a) 1Aol, (b) 2Aol, and (c) 2M2Aol. (d)–(f) Pressure-dependent transition entropy changes on heating (red data) and cooling (blue data) for (d) 1Aol, (e) 2Aol, and (f) 2M2Aol. Lines are fits to the data. (g)–(i) Temperature-pressure phase diagram on heating (red data) and cooling (blue data) for (g) 1Aol, (h) 2Aol, and (i) 2M2Aol. The shadowed area is limited by the onset temperature (thick line) and the peak maximum temperature. The dashed horizontal green line indicates the endothermic transition temperature at atmospheric pressure, and the dashed vertical line indicates the pressure at which the exothermic transition temperature is equal to the normal pressure endothermic transition temperature, which is the minimum pressure, p_{rev} required to obtain reversible barocaloric effects.

TABLE I. Properties of phases at atmospheric pressure for the compounds investigated in this work. Values for $\left(\frac{\partial V}{\partial T}\right)_p$ and α are calculated in the vicinity of the transition. For 2AoI, the two values for α in phase M are calculated close to the transitions Tr–M and M-FCC, respectively.

Compound	Chemical formula	Phase	Space group	Z	$\left(\frac{\partial V}{\partial T}\right)_p$ m^3 kg^{-1} K^{-1}	$\alpha(\cdot 10^4)$ K^{-1}	References
1-Adamantanol	$C_{10}H_{16}O$	FCC	$Fm\bar{3}m$	4	3.2×10^{-7}	3.60	This work
		T	$P4_2/n$	8	1.6×10^{-7}	1.89	This work
2-Adamantanol	$C_{10}H_{16}O$	FCC	$Fm\bar{3}m$	4	4.4×10^{-7}	4.4	This work,[35]
		M	$C2/m$	12	3.1×10^{-7}	3.1–3.2	35
		Tr	$P\bar{1}$	6	2.7×10^{-7}	2.8	35
2-Methyl-2-adamantanol	$C_{11}H_{18}O$	FCC	$Fm\bar{3}m$	4	5.2×10^{-7}	4.09	This work,[35]
		O	$Pbcn$	16	1.9×10^{-7}	2.02	35

in the transition. In the plastic phase, the Rietveld refined structures from XRPD yielded the $Fm\bar{3}m$ space group with Z = 4 for the three compounds under study, in contrast to F43c, $F\bar{4}3$m and F43c previously assigned by other works to 1AoI,[36] 2AoI,[36] and 2M2AoI,[37] respectively. The resulting 48 possible molecular orientations allowed by this symmetry[45] and considering a single molecular conformation due to the rigid character of the fused rings[46] give rise to $N_{FCC} = 48$ configurations. In phase O, 2M2AoI is completely ordered ($N_O = 1$),[35] resulting in $\Delta S^c_{O\to FCC} \simeq 194$ J K^{-1} kg^{-1}. As for this compound $\Delta S^V_{O\to FCC}$ ~110 J K^{-1} kg^{-1}, we obtain $\Delta S^c_{O\to FCC} + \Delta S^V_{O\to FCC} \sim 304$ J K^{-1} kg^{-1}, which is below our measured value (see Table II). This difference may be due to the large uncertainty involved in the estimation of ΔS^V or to additional contributions arising, for instance, from non-volumic strains. In any case, it is apparent that for 2M2AoI, the volumic entropy change is comparable to the configurational entropy change and consistent with the general trend observed in some plastic crystals, according to which $\Delta S^V \sim 0.4\Delta S_t$.[47]

For 1AoI, in phase T, the hydrogen of the hydroxyl group is disordered between two positions,[35] giving rise to $N_T = 2$. This results in a $\Delta S^c_{T\to FCC} \simeq 174$ J K^{-1} kg^{-1}. Given that for this compound $\Delta S^V_{T\to FCC} \sim 40$ J K^{-1} kg^{-1}, the sum of the two entropic contributions yields $\Delta S^c_{T\to FCC} + \Delta S^V_{T\to FCC} \sim 214$ J K^{-1} kg^{-1}, which is in good agreement with the measured total entropy change, so that we can conclude that the main contribution in this case emerges from the orientational disorder.

In 2AoI, the configurational disorder emerges progressively across a series of phase transitions (see Sec. I). In phase Tr, the disorder of H atoms between two different positions yields $N_{Tr} = 2$, whereas in phase M, the additional disorder in O atoms, also between two possible sites,[35] yields $N_M = 4$. This results in $\Delta S^c_{Tr\to M} \simeq 38$ J K^{-1} kg^{-1}. This is much higher than our measured total entropy change, which can be ascribed to the fact that the mentioned disorder can arise progressively in temperature within the phases and not strictly at the phase transitions, in accordance with the evident pre-transitional effects reflected in a strong increase in the specific heat around 30 K before the Tr → M transition.[36] In turn, we estimate a small $\Delta S^V_{Tr\to M} \sim 3$ J K^{-1} kg^{-1}. As for the M → FCC transition, from the above considerations we obtain $\Delta S^V_{M\to FCC} \simeq 136$ J K^{-1} kg^{-1}, which is one order of magnitude higher than our measured total

TABLE II. Thermodynamic properties at the endothermic and exothermic phase transitions under study. Values for $\frac{d(\Delta S_t)}{dp}$ correspond to the endothermic transition in all cases. ΔV_t stands for volume changes at the transition determined from x-ray diffraction, whereas ΔV_t^{CC} refers to values calculated using the Clausius–Clapeyron equation at the endothermic transition.

	1AoI		2AoI				2M2AoI	
	T → FCC	FCC → T	Tr → M	M → Tr	M → FCC	FCC → M	O → FCC	FCC → O
T_0 (K)	360 ± 1	348 ± 1	325 ± 1	327 ± 1	389 ± 1	389 ± 1	371 ± 1	367 ± 1
T_t (K)	361 ± 1	346 ± 1	326 ± 1	324 ± 1	390 ± 1	389 ± 1	375 ± 1	364 ± 1
$\frac{dT}{dp}$ (K GPa^{-1})	179 ± 5	154 ± 5	210 ± 10	207 ± 8	48 ± 1	53 ± 1	241 ± 1	222 ± 1
ΔH_t (kJ kg^{-1})	75.4 ± 1	70.9 ± 1	4.2 ± 0.3	6.2 ± 0.4	25.9 ± 1.5	26.2 ± 1.5	137 ± 6	127 ± 6
ΔS_t (J K^{-1} kg^{-1})	210 ± 10	207 ± 10	12.9 ± 1	19.5 ± 1	66.5 ± 4	66.7 ± 4	371 ± 13	357 ± 10
$d(\Delta S_t)/dp$ (J K^{-1} kg^{-1})	−0.25 ± 0.01		0.017 ± 0.004		−0.11 ± 0.01		−0.15 ± 0.08	
ΔV_t (cm^3 g^{-1})	(4.5 ± 0.5)·10^{-2}		(0.27 ± 0.04)·10^{-2}		(0.54 ± 0.14)·10^{-2}		(8.8 ± 0.9)·10^{-2}	
ΔV_t^{CC} (cm^3 g^{-1})	(3.8 ± 0.5)·10^{-2}		(0.27 ± 0.05)·10^{-2}		(0.32 ± 0.06)·10^{-2}		(8.4 ± 0.8)·10^{-2}	

entropy change. The origin of such a huge discrepancy must have its origin in the partial activation of the orientational degrees of freedom at the M → FCC phase transition. Actually, our Rietveld refinement is also consistent with $N_{FCC} = 24$ configurations, which would yield a value of $\Delta S^{c}_{M\rightarrow FCC} \simeq 98$ J K^{-1} kg^{-1}, still higher but closer to the measured one. In turn, the volumic entropy change is estimated to be small, $\Delta S^{V}_{M\rightarrow FCC} \sim 7$ J K^{-1} kg^{-1}.

We now turn to analyzing the dependence of the thermodynamic properties on pressure [see Figs. 1(d)–1(f) and Table I]. When increasing pressure, a clear decrease of ΔS_t was obtained for the T ↔ FCC and M ↔ FCC transitions in 1AoI and 2AoI, respectively, which is a behavior obtained in other ordered-to-plastic crystal transitions.[4,48] For the O-FCC transition in 2M2AoI, a large dispersion for ΔS_t was obtained, resulting in a slight dependence on pressure on average. For the Tr–M transition in 2AoI, the ΔS_t was obtained to be nearly independent of pressure within the pressure range under study. This overall behavior could be ascribed to the high compressibility of plastic phases as suggested by Li *et al.*,[49] which would make the transition volume change decrease at higher pressure, with a consequent reduction of the volumic entropy change. As in any case, the volumic entropy change is insignificant for the Tr–M transition in 2AoI, ΔS_t for this transition is unaffected by pressure.

Onset and peak maximum temperatures were determined from the peak positions, and their dependence on pressure enabled to determine the phase diagram and the slope of the transition line $\frac{dT}{dp}$ [see Figs. 1(g)–1(i) and Table II] for both the endothermic (in equilibrium) and exothermic (out of equilibrium) transitions. In the case of 2AoI, the fact that $\frac{dT_{Tr\rightarrow M}}{dp} > \frac{dT_{M\rightarrow FCC}}{dp}$ at any pressure within the range under analysis points toward the existence of a triple point Tr–M–FCC, beyond which phase M becomes metastable. Performing a second-order polynomial fit to the $T(p)$ data for the two transitions, the coordinates of the triple point are estimated as $(T,p)_{Tr-M-FCC} \sim$ (410 K, 490 MPa).

As discussed in the introduction, determining the transition hysteresis, i.e., differences between endothermic and exothermic transition temperatures, may be key for applications, either as a drawback or as an advantage. For BC cooling or heat pumping cycles, it has been shown that the hysteresis introduces a minimum pressure threshold, p_{rev}, required to obtain reversible adiabatic temperature changes, ΔT_{rev}. The value for p_{rev} can be determined as the value for which the exothermic transition temperature equals the endothermic transition temperature at atmospheric pressure.[38] Values are indicated in Figs. 1(g)–1(i).

It is therefore clear that, given a certain thermal hysteresis, the larger the $\frac{dT}{dp}$ the lower the p_{rev}. Moreover, a large $\frac{dT}{dp}$ is also desirable because it enhances the adiabatic temperature changes ΔT. Nevertheless, the value for $\frac{dT}{dp}$ is inversely proportional to the value for ΔS_t as required by the Clausius–Clapeyron (CC) equation, $\frac{dT}{dp} = \frac{\Delta V_t}{\Delta S_t}$, and ΔS_t is also desired to be large to obtain large isothermal entropy changes ΔS. As both quantities ΔT and ΔS are the key quantities for BC cooling or heat pumping, a trade-off is sought. Interestingly, for 1AoI and 2M2AoI both ΔS_t and $\frac{dT}{dp}$ displayed for the III transitions between a (semi)ordered and the plastic phases are simultaneously large. This win–win situation is due to the huge transition volume changes ΔV_t, as linked by the same CC equation. In fact, the CC equation was used to estimate the transition volume changes, which were found to be in reasonable agreement with the experimental value obtained in this work for 1AoI and experimental values available in the literature[35] for 2AoI and 2M2AoI, except for the M → FCC transition in 2AoI (see Table II and the supplementary material).

B. Determination of barocaloric responses

Our isobaric high-pressure calorimetry measurements allowed us to calculate the BC effects using the quasi-direct method.[50] Accordingly, the isobaric temperature-dependent entropy $S(T,p)$ is calculated with respect to a reference temperature T_0 and atmospheric pressure, $S(T_0,p_{atm})$, using a TdS equation extended to include the heat flow contribution arising from the first-order phase transition,

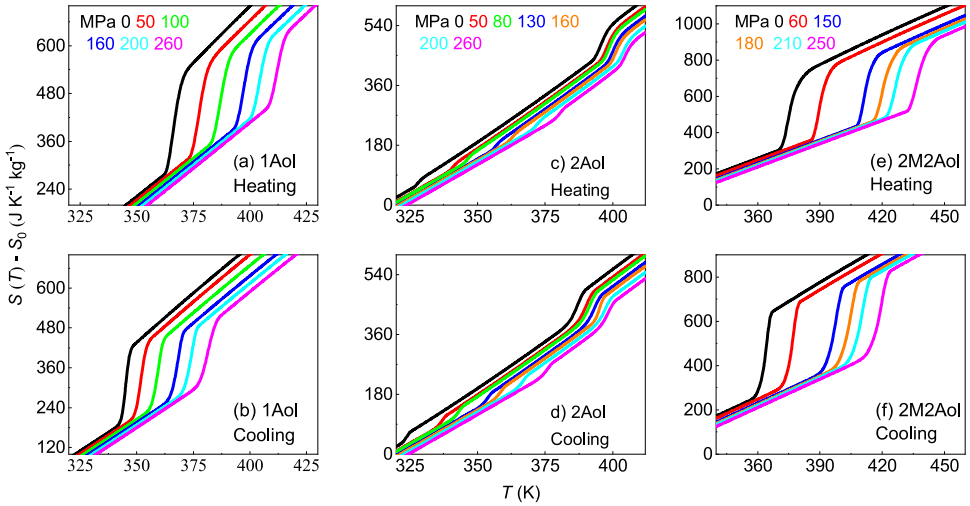

FIG. 2. Isobaric entropy curves at selected pressures with respect to a reference value $S_0 \equiv S(T_0, p_{atm})$, on heating (top panels) and cooling (bottom panels) for (a), (b) 1AoI, (c), (d) 2AoI, and (e), (f) 2M2AoI. The color legend for pressure values in the top panels is also valid in the corresponding bottom panels.

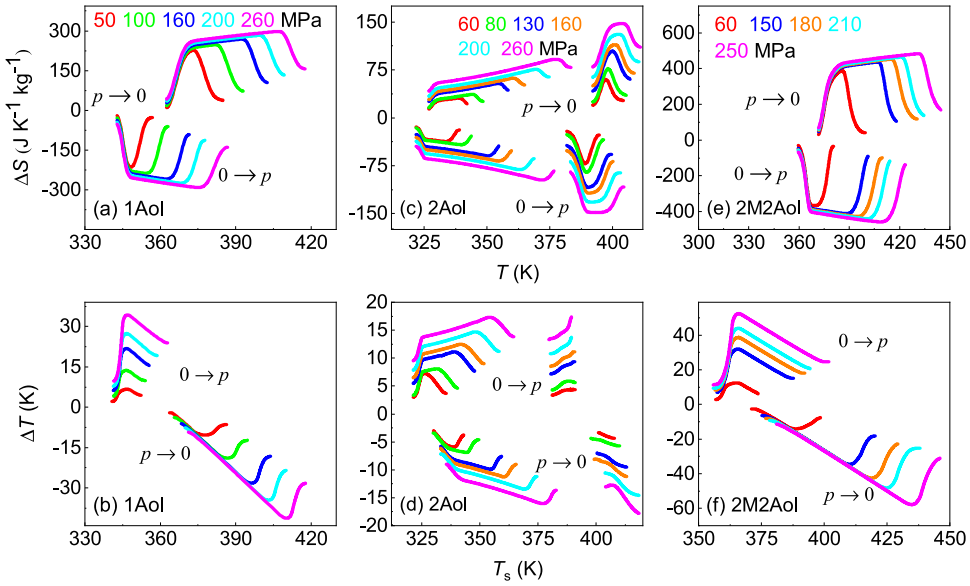

FIG. 3. Isothermal entropy changes ΔS and adiabatic temperature changes ΔT in (a), (b) 1AoI, (c), (d) 2AoI, and (e), (f) 2M2AoI, respectively, obtained upon the first application and removal of pressure. Notice that ΔT is conveniently plotted as a function of the starting temperature T_s of the heating/cooling process.

$$S(T,p) - S(T_0,p_{atm}) = \int_{T_0}^{T} \frac{C_p}{T} dT - \int_{p_{atm}}^{p} \left(\frac{\partial V}{\partial T}\right)_{p;T_0} dp + \int_{T_i}^{T} \frac{1}{T} \frac{dQ(p,T)}{|dT|} dT.$$

Here, we used T_0 = 300 K for 1AoI, T_0 = 315 K for 2AoI, and T_0 = 340 K for 2M2AoI, and T_i is a pressure dependent temperature chosen to properly take into account the heat flow associated with the transition. In turn, the pressure- and temperature-dependent heat capacity $C_p(T,p)$ was constructed using data at atmospheric pressure from literature.[36,37] As the transition temperature range depends on the applied pressure, the heat capacity was extrapolated in temperature accordingly. Moreover, in each phase within the temperature range under analysis, the heat capacity could be considered independent of pressure within error as entailed by the linear temperature dependence of volume (see the supplementary material and Ref. 35) and the equation $\left(\frac{\partial C_p}{\partial p}\right)_T = -T\left(\frac{\partial^2 V}{\partial T^2}\right)_p$. Notice that this does not contradict the fact that the heat capacity may (and actually must) depend on pressure at lower temperature ranges where volume is surely not linearly dependent on temperature. This

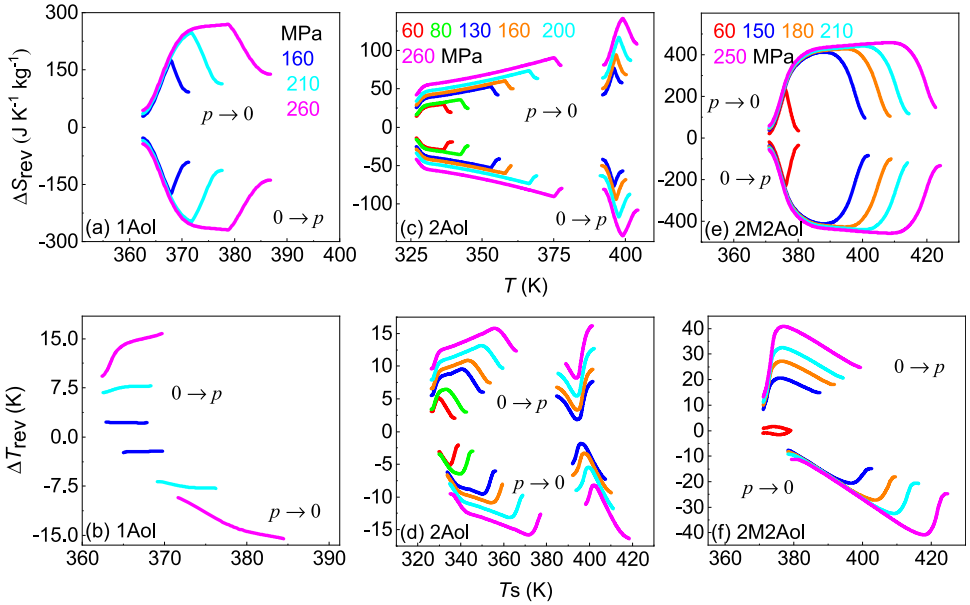

FIG. 4. Reversible isothermal entropy changes ΔS_{rev} and adiabatic temperature changes ΔT_{rev} for (a), (b) 1AoI, (c), (d) 2AoI, and (e), (f) 2M2AoI, respectively, obtained upon cyclic pressure changes.

lower-temperature dependence of C_p causes the entropy of each phase to depend on pressure at higher temperatures, and in particular within the temperature ranges of interest for this work. This dependence of the entropy is reflected by the existence of the term containing $\left(\frac{\partial V}{\partial T}\right)_p$ in the previous equation. In turn, we assume that $\left(\frac{\partial V}{\partial T}\right)_p$ is independent of pressure so that $\int_{p_{atm}}^{p}(\partial V/\partial T)_p dp \simeq \left(\frac{\partial V}{\partial T}\right)_{p_{atm}}(p - p_{atm})$. This assumption has been found to be reasonable for other plastic crystals.[4] For 1AoI, this term was calculated from $V(T)$ data obtained from temperature-dependent XRPD measurements (see Figs. S4 and S5). For 2AoI and 2M2AoI, $\left(\frac{\partial V}{\partial T}\right)_{p_{atm}}$ was calculated from $V(T)$ literature data.[35] The corresponding values are included in Table I. On the other hand, obtaining these data at high pressure is experimentally difficult and overall introduces only small errors in the calculation of the entropy curves and the subsequent barocaloric effects within the pressure range considered in this work. In particular, an uncertainty of about 20% in the value of $\left(\frac{\partial V}{\partial T}\right)_p$ entails an uncertainty of <2% of the maximum ΔS and <1% of the maximum ΔT for a pressure change of 105 MPa in 1AoI, of ~9% of the maximum ΔS and <18% of the maximum ΔT for a pressure change of 150 MPa in 2AoI and of ~1.3% of the maximum ΔS and <0.5% of the maximum ΔT for a pressure change of 110 MPa in 2M2AoI. The resulting entropy functions are shown in Fig. 2.

Subsequently, BC effects were determined by subtracting the entropy curves following the procedure explained in Ref. 38. First, we calculated the isothermal entropy changes ΔS and adiabatic temperature changes ΔT that can be obtained on the first application or removal of pressure (see Fig. 3). Despite the fact that these effects are irreversible when the pressure change is directly reversed, they could be used for applications for pressure-driven waste heat management, as discussed in the introduction. The obtained results reveal colossal values at moderate pressure changes for all of them, as previously obtained for other plastic crystals.[5,38,48,49] It is remarkable that 1AoI exhibits $\Delta S \sim 220$ J K^{-1} kg^{-1} and $\Delta T \sim 10$ K under small pressure changes of 50 MPa that increase up to 300 J K^{-1} kg^{-1} and $\Delta T \sim 40$ K under pressure changes of 250 MPa; 2M2AoI displays $\Delta S \sim 360$ J K^{-1} kg^{-1} and $\Delta T \sim 10$ K under small pressure changes of 60 MPa that increase up to 450 J K^{-1} kg^{-1} and $\Delta T \sim 40$ K under

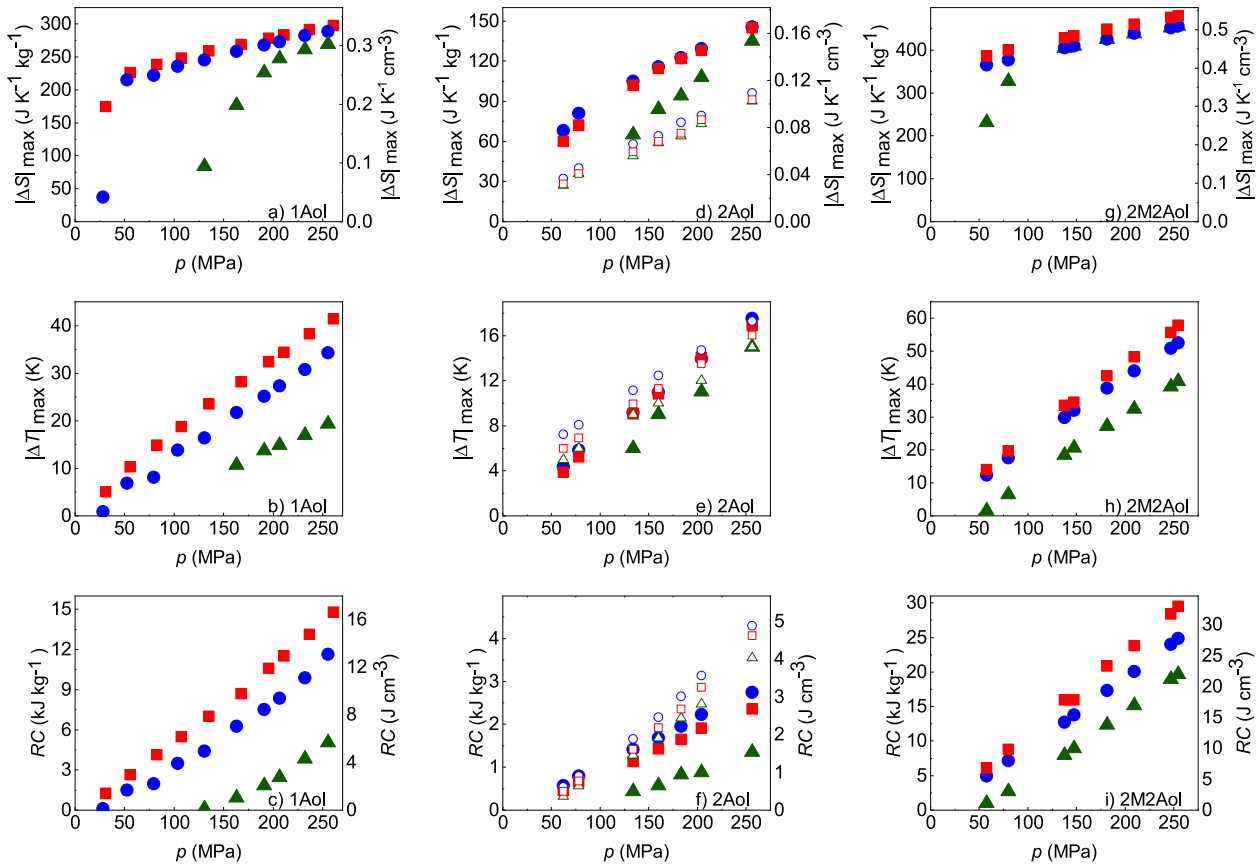

FIG. 5. Maximum isothermal entropy changes (a), (d), (g) per unit mass (left axis) and per unit volume (right axis), adiabatic temperature changes (b), (e), (h) and refrigerant capacity (c), (f), (i) for 1AoI (a)–(c), 2AoI (d)–(f), and 2M2AoI (g)–(i) upon first application (blue) and removal (red) of pressure and upon reversible pressure changes (green) as a function of pressure change, obtained across the T–FCC, M–FCC, and O–T transitions for 1AoI, 2AoI, and 2M2AoI, respectively (solid symbols), and across the Tr–M transition for 2AoI (empty symbols).

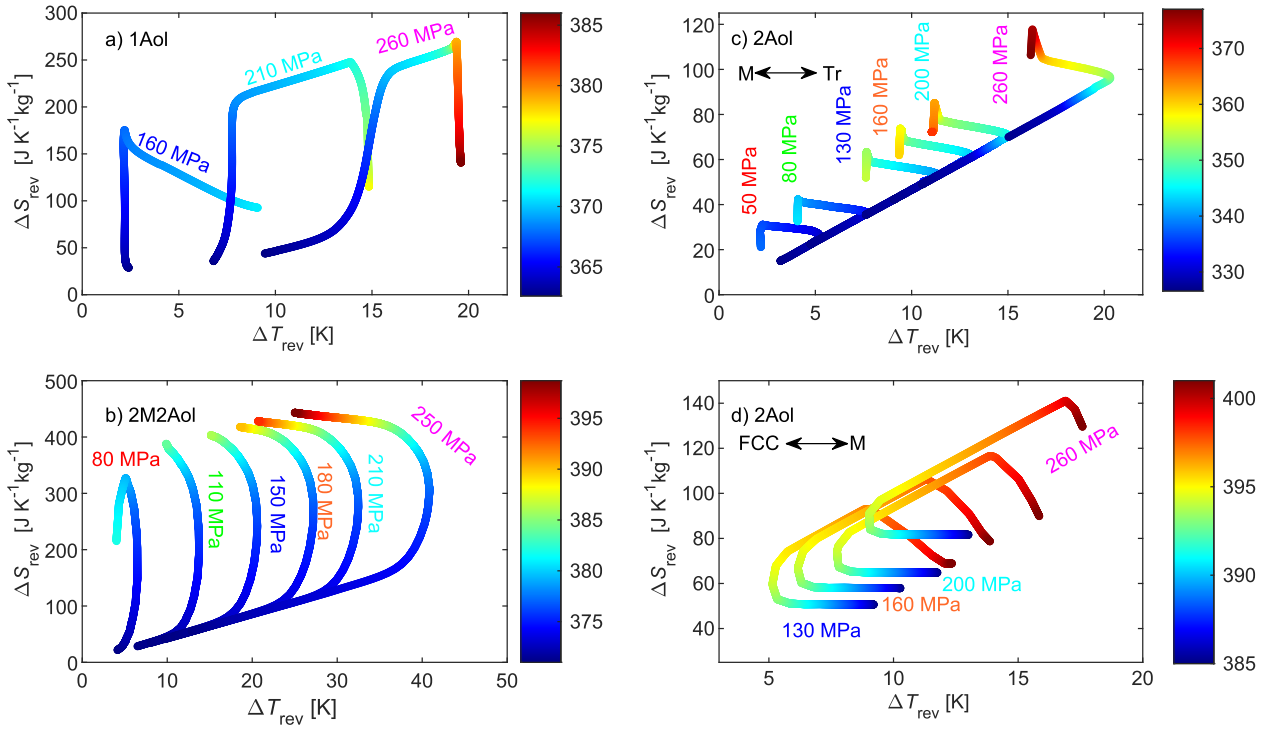

FIG. 6. Reversible adiabatic temperature changes and isothermal entropy changes that can be obtained at different applied pressure changes occurring at temperatures indicated by the color code.

pressure changes of 250 MPa; 2AoI reaches $\Delta S \sim 100$ J K^{-1} kg^{-1} and $\Delta T \sim 10$ K at 140 MPa, which are smaller values compared to 1AoI and 2M2AoI. However, the two transitions Tr → M and M → FCC in 2AoI each provide a temperature window where significant BC effects are obtained, thus resulting in two temperature intervals of operation. It is worth noting here that, for this compound, the contribution of the thermal expansion to ΔS has a significant relative weight, amounting to ~50% of the total ΔS

TABLE III. Summary of barocaloric properties of 1AoI, 2AoI, and 2M2AoI and comparison with other colossal BC materials near pressure changes Δp for which $\Delta S_{rev} \gtrsim 100$ J K^{-1} kg^{-1} are reported. ∗Values obtained at a melting transition. Values for irreversible ΔS have been averaged over the application and removal of pressure.

	ΔS J K^{-1} kg^{-1}	Δp MPa	ΔS_{rev} J K^{-1} kg^{-1}	ΔT_{rev} K	Δp MPa	References
1-Adamantanol	220	50	175	11	160	This work
2-Adamantanol	100	120	~100	8	185	This work
2-Methyl-2-adamantanol	360	60	300	7	80	This work
$(CH_3)_2C(CH_2OH)_2$	370	50	421	7.5	250	5
$(CH_3)C(CH_2OH)_3$	300	40	490	10	240	38
$(CH_3)_3C(CH_2OH)$	250	100	293	16	260	38
$(NH_2)CH_3(CH_2OH)_2$	600	100	...	...	...	38
$(NH_2)C(CH_2OH)_3$	330	50	...	...	...	38
$C_{10}H_{15}Cl$	140	20	115	5	50	48
$C_{10}H_{15}Br$	120	50	110	7	50	48
Acetoxy silicone rubber	150	87	182	21	173	51
$Fe_3(bntrz)_6(tcnset)_6$	80	33	100	~22	120	52
$Fe[HB(tz)_3]_2$	75	4	89	1.7	12	53
$(C_{10}H_{21}NH_3)_2MnCl_4$	250	30	230	5	50	54
$C_2B_{10}H_{12}$	100	30	~100	...	50	55
MIL-53(Al)	...	...	311	...	1.6	56
$C_{16}H_{34}$*	600	22	~700	8	50	57

at 200 MPa. Finally, we calculated the reversible BC effects that are obtained upon cyclic application and removal of pressure (see Fig. 4). Maximum values as a function of pressure for both irreversible and reversible effects along with refrigerant capacity[48] (RC) are shown in Fig. 5, and joint values for ΔS_{rev} and ΔT_{rev} are plotted in Fig. 6 for different applied pressure changes as a function of temperature. Consistently with the values previously calculated for p_{rev} from the endothermic and exothermic transition lines $T(p)$, our results reveal that 1AoI exhibits non-zero ΔS_{rev} from ~130 MPa, which becomes colossal around 150 MPa. 2AoI exhibits reversible BC effects from ~60 MPa at the Tr–M transition and from ~140 MPa at the M–C transition and becomes colossal under higher pressure changes of ~185 MPa. Again, 2M2AoI outperforms 1AoI and 2AoI, displaying colossal $\Delta S_{rev} \sim 300$ J K^{-1} kg^{-1} and $\Delta T_{rev} \sim 7$ K upon pressure changes of 80 MPa. A comparison of the BC response for 1AoI, 2AoI, and 2M2AoI along with other solid-state materials exhibiting colossal BC effects is shown in Table III. Irreversible ΔT values are not included because they are not figures of merit for waste heat management.

IV. CONCLUSIONS

In this work, we have characterized the barocaloric response of three plastic crystals formed by hydroxyl derivatives of adamantane across their solid–solid first-order phase transitions. For this purpose, we have performed x-ray powder diffraction and custom-built pressure-dependent calorimetry, with which we have determined the pressure dependence of thermodynamic properties at the endothermic and exothermic transitions. Based on calculated isobaric temperature-dependent entropy at different pressures, the barocaloric effects have been calculated using the quasi-direct method. Overall, we found that colossal isothermal entropy changes well above 100 J K^{-1} kg^{-1} can be obtained irreversibly under moderate pressure changes of 60–150 MPa and reversibly upon pressure changes of ~100–200 MPa, depending on the compound. In particular, it is worth emphasizing that 2-methyl-2-adamantanol reaches irreversible effects of 360 J K^{-1} kg^{-1} under 60 MPa pressure changes and reversible effects of 300 J K^{-1} kg^{-1} and 7 K under 80 MPa pressure changes, and 430 J K^{-1} kg^{-1} and 40 K under 250 MPa. The origin for this colossal barocaloric response for this compound relies on the release of the orientational degrees of freedom and a very large volume change at the transition, contributing with the same order of magnitude to the total transition entropy change ΔS_t. For the other compounds, it is estimated that at the transition, the contribution of the orientational disordering is dominant over the purely volumic entropy change. Moreover, for 1-adamantanol and 2-methyl-2-adamantanol, the very large volume change permits both ΔS and ΔT be simultaneously large, despite the counteraction of their main contributions (ΔS_t and $\frac{dT}{dp}$) in the Clausius–Clapeyron equation.

This work expands the library of colossal barocaloric plastic crystals. The transition temperatures lying above room temperature make these materials unsuited for household applications but could be suited for pressure-assisted thermal energy storage as well as in the industrial sector for heat pumping and high-temperature cooling.

SUPPLEMENTARY MATERIAL

See the supplementary material file for the XRPD patterns of the plastic phases of 1AoI, 2AoI, and 2M2AoI, ordered phase of 1AoI, with tables containing the experimental angular positions obtained for the Bragg peaks from Rietveld refinement, refined crystal structure for the ordered phase of 1AoI, temperature-dependent XRPD patterns, lattice parameters, and unit-cell volume for 1AoI.

ACKNOWLEDGMENTS

This work was supported by MINECO Project No. PID2020-112975GB-I00 (Spain) and DGU Project No. 2017SGR-42 (Catalonia).

AUTHOR DECLARATIONS

Conflict of Interest

Josep-Lluís Tamarit and Pol Lloveras have Patent No. PCT/EP 2017/076203 licensed.

Author Contributions

Alejandro Salvatori: Formal analysis (equal); Investigation (equal); Visualization (equal); Writing – review & editing (supporting). **Philippe Negrier**: Formal analysis (equal); Investigation (equal); Methodology (equal); Validation (equal); Visualization (equal); Writing – review & editing (equal). **Araceli Aznar**: Formal analysis (equal); Investigation (equal); Validation (equal); Writing – review & editing (supporting). **María Barrio**: Formal analysis (equal); Investigation (equal); Methodology (equal); Project administration (equal); Validation (equal); Visualization (equal); Writing – review & editing (equal). **Josep Lluís Tamarit**: Conceptualization (lead); Funding acquisition (lead); Investigation (supporting); Methodology (lead); Project administration (lead); Resources (lead); Supervision (lead); Validation (equal); Writing – review & editing (equal). **Pol Lloveras**: Conceptualization (equal); Formal analysis (equal); Investigation (equal); Methodology (equal); Supervision (equal); Validation (equal); Visualization (equal); Writing – original draft (lead); Writing – review & editing (equal).

DATA AVAILABILITY

The data that support the findings of this study are available from the corresponding author upon reasonable request.

REFERENCES

[1] J. Timmermans, J. Phys. Chem. Solids **18**, 1 (1961).
[2] B. Alefeld, N. Parsonage, and L. Staveley, "Disorder in crystals," *International Series of Monographs on Chemistry* (Clarendon University Press, Oxford, 1980).
[3] J. L. Tamarit, B. Legendre, and J. M. Buisine, Mol. Cryst. Liq. Cryst. **250**, 347 (1994).
[4] A. Aznar, P. Lloveras, M. Barrio, and J.-L. Tamarit, Eur. Phys. J.: Spec. Top. **226**, 1017 (2017).

[5]P. Lloveras, A. Aznar, M. Barrio, P. Negrier, C. Popescu, A. Planes, L. Mañosa, E. Stern-Taulats, A. Avramenko, N. D. Mathur, X. Moya, and J.-L. Tamarit, Nat. Commun. **10**, 1803 (2019).
[6]P. Lloveras and J.-L. Tamarit, MRS Energy Sustainability **8**, 3 (2021).
[7]See https://www.waste-heat.eu/ for an overview of waste heat resources and opportunities in Europe; accessed May 2022.
[8]See https://arpa-e.energy.gov/technologies/projects/closed-loop-system-using-waste-heat-electricity for opportunities on waste heat reuse; accessed May 2022.
[9]See https://arpa-e.energy.gov/technologies/projects/waste-heat-recovery-system for information about low-temperature waste heat potential; accessed May 2022.
[10]See https://e360.yale.edu/features/waste-heat-innovators-turn-to-an-overlooked-renewable-resource for an overview on waste heat opportunities; accessed May 2022.
[11]H. Jouhara, N. Khordehgah, S. Almahmoud, B. Delpech, A. Chauhan, and S. A. Tassou, Therm. Sci. Eng. Prog. **6**, 268 (2018).
[12]A. Jamekhorshid, S. M. Sadrameli, and M. Farid, "A review of microencapsulation methods of phase change materials (PCMs) as a thermal energy storage (TES) medium," Renewable Sustainable Energy Rev. **31**, 531 (2014).
[13]A. Serrano, J.-L. Dauvergne, S. Doppiu, and E. Palomo Del Barrio, Materials **12**, 3169 (2019).
[14]M. Barrio, J. Font, D. O. López, J. Muntasell, and J. L. Tamarit, Sol. Energy Mater. Sol. Cells **27**, 127 (1992).
[15]H. Tokoro, M. Yoshikiyo, K. Imoto, A. Namai, T. Nasu, K. Nakagawa, N. Ozaki, F. Hakoe, K. Tanaka, K. Chiba, R. Makiura, K. Prassides, and S.-I. Ohkoshi, Nat. Commun. **6**, 7037 (2015).
[16]S.-i. Ohkoshi, H. Tokoro, K. Nakagawa, M. Yoshikiyo, F. Jia, and A. Namai, Sci. Rep. **9**, 13203 (2019).
[17]A. Moldgy and R. Parameshwaran, "Study on thermal energy storage properties of organic phase change material for waste heat recovery applications," in *International Conference on Advanced Materials (SCICON '16), December 19–21, 2016* [Mater. Today: Proc. **5**, 16840–16848 (2018)].
[18]J. Z. Alvi, Y. Feng, Q. Wang, M. Imran, and G. Pei, Energy **223**, 120006 (2021).
[19]J. Font and J. Muntasell, Mater. Res. Bull. **29**, 1091 (1994).
[20]J. G. Aston, *Physics and Chemistry of the Organic Solid State* (Interscience, New York, 1994), Vol. 1, pp. 543–583.
[21]C. E. Nordman and D. L. Schmitkons, Acta Crystallogr. **18**, 764 (1965).
[22]P. Negrier, M. Barrio, M. Romanini, J. L. Tamarit, D. Mondieig, A. I. Krivchikov, L. Kepinski, A. Jezowski, and D. Szewczyk, Cryst. Growth Des. **14**, 2626 (2014).
[23]P. Negrier, M. Barrio, J. L. Tamarit, and D. Mondieig, J. Phys. Chem. B **118**, 9595 (2014).
[24]L. Yuan, S. Clevers, A. Burel, P. Negrier, M. d. Barrio, B. Ben Hassine, D. Mondieig, V. Dupray, J. L. Tamarit, and G. Coquerel, Cryst. Growth Des. **17**, 3395 (2017).
[25]P. Negrier, B. B. Hassine, M. Barrio, M. Romanini, D. Mondieig, and J.-L. Tamarit, "Polymorphism of 1,3-X-adamantanes (X = Br, OH, CH_3) and the crystal plastic phase formation ability," CrystEngComm **22**, 1230 (2020).
[26]J. P. Amoureux, M. Bee, C. Gors, V. Warin, and F. Baert, "1-adamantanol, $C_{10}H_{16}O$," Cryst. Struct. Comm. **8**, 449 (1979).
[27]K. Mitsukura, H. Sakamoto, H. Kubo, T. Yoshida, and T. Nagasawa, J. Biosci. Bioeng. **109**, 550 (2010).
[28]N. Tanaka and M. Yamaguchi, "Method for producing 1,3-adamantanediol," JP2005082563A, 2003.
[29]A. Orzeszko, B. Kamińska, and B. J. Starościak, Il Farmaco **57**, 619 (2002).
[30]K. Nozaki, K. Watanabe, E. Yano, A. Kotachi, S. Takechi, and I. Hanyu, J. Photopolym. Sci. Technol. **9**, 509 (1996).
[31]K. Aigami, Y. Inamoto, N. Takaishi, K. Hattori, A. Takatsuki, and G. Tamura, J. Med. Chem. **18**, 713 (1975).
[32]J. M. Rabey, P. Nissipeanu, and A. D. Korczyn, J. Neural Transm.: Parkinson's Dis. Dementia Sect. **4**, 277 (1992).
[33]J. S. Wishnok, J. Chem. Educ. **50**, 780 (1973).
[34]See http://www.accelrys.com for MS modeling (Materials Studio), version 5.5.
[35]A. Salvatori, P. Negrier, S. Massip, A. Muñoz-Duque, P. Lloveras, M. Barrio, and J.-L. Tamarit, CrystEngComm **24**, 3692 (2022).
[36]M. B. Charapennikau, A. V. Blokhin, A. G. Kabo, and G. J. Kabo, J. Chem. Thermodyn. **35**, 145 (2003).
[37]M. B. Charapennikau, A. V. Blokhin, G. J. Kabo, A. G. Kabo, V. V. Diky, and A. G. Gusakov, Thermochim. Acta **382**, 109 (2002).
[38]A. Aznar, P. Lloveras, M. Barrio, P. Negrier, A. Planes, L. Mañosa, N. D. Mathur, X. Moya, and J.-L. Tamarit, J. Mater. Chem. A **8**, 639 (2020).
[39]R. Sandrock and G. M. Schneider, Ber. Bunsenges. Phys. Chem. **87**, 197 (1983).
[40]M. Jenau, J. Reuter, J. L. Tamarit, and A. Würflinger, J. Chem. Soc., Faraday Trans. **92**, 1899 (1996).
[41]E. L. Gromnitskaya, I. V. Danilov, and V. V. Brazhkin, Phys. Chem. Chem. Phys. **23**, 2349 (2021).
[42]J. R. Drabble and A. H. M. Husain, J. Phys. C **13**, 1377 (1980).
[43]J. C. Damien, Solid State Commun. **16**, 1271 (1975).
[44]E. L. Gromnitskaya, I. V. Danilov, and V. V. Brazhkin, Phys. Chem. Chem. Phys. **24**, 18022 (2022).
[45]J. P. Amoureux and M. Bee, Acta Crystallogr. **35**, 2957 (1979).
[46]J. P. Amoureux, M. Bee, and J. C. Damien, Acta Crystallogr. **36**, 2633 (1980).
[47]G. J. Kabo, A. A. Kozyro, M. Frenkel, and A. V. Blokhin, Mol. Cryst. Liq. Cryst. **326**, 333 (1999).
[48]A. Aznar, P. Negrier, A. Planes, L. Mañosa, E. Stern-Taulats, X. Moya, M. Barrio, J.-L. Tamarit, and P. Lloveras, Appl. Mater. Today **23**, 101023 (2021).
[49]B. Li, Y. Kawakita, S. Ohira-Kawamura, T. Sugahara, H. Wang, J. Wang, Y. Chen, S. I. Kawaguchi, S. Kawaguchi, K. Ohara, K. Li, D. Yu, R. Mole, T. Hattori, T. Kikuchi, S.-I. Yano, Z. Zhang, Z. Zhang, W. Ren, S. Lin, O. Sakata, K. Nakajima, and Z. Zhang, Nature **567**, 506 (2019).
[50]L. Mañosa and A. Planes, Adv. Mater. **29**, 1603607 (2017).
[51]W. Imamura, É. O. Usuda, L. S. Paixão, N. M. Bom, A. M. Gomes, and A. M. G. Carvalho, Chin. J. Polym. Sci. **38**, 999 (2020).
[52]M. Romanini, Y. Wang, K. Gürpinar, G. Ornelas, P. Lloveras, Y. Zhang, W. Zheng, M. Barrio, A. Aznar, A. Gràcia-Condal, B. Emre, O. Atakol, C. Popescu, H. Zhang, Y. Long, L. Balicas, J. Lluís Tamarit, A. Planes, M. Shatruk, and L. Mañosa, Adv. Mater. **33**, 2008076 (2021).
[53]J. Seo, J. D. Braun, V. M. Dev, and J. A. Mason, J. Am. Chem. Soc. **144**, 6493 (2022).
[54]J. Li, M. Barrio, D. J. Dunstan, R. Dixey, X. Lou, J. L. Tamarit, A. E. Phillips, and P. Lloveras, Adv. Funct. Mater. **31**, 2105154 (2021).
[55]K. Zhang, R. Song, J. Qi, Z. Zhang, Z. Zhang, C. Yu, K. Li, Z. Zhang, and B. Li, Adv. Funct. Mater. **32**, 2112622 (2022).
[56]J. García-Ben, J. López-Beceiro, R. Artiaga, J. Salgado-Beceiro, I. Delgado-Ferreiro, Y. V. Kolen'ko, S. Castro-García, M. A. Señarís-Rodríguez, M. Sánchez-Andújar, and J. M. Bermúdez-García, Chem. Mater. **34**, 3323 (2022).
[57]J. Lin, P. Tong, K. Zhang, K. Tao, W. Lu, X. Wang, X. Zhang, W. Song, and Y. Sun, Nat. Commun. **13**, 596 (2022).